RSC Advances

PAPER

View Article Online
View Journal | View Issue

Cite this: *RSC Adv.*, 2020, **10**, 25517

Design, synthesis, and biological evaluation of new 6,N^2-diaryl-1,3,5-triazine-2,4-diamines as anticancer agents selectively targeting triple negative breast cancer cells†

Ahmad Junaid,[a] Felicia Phei Lin Lim,[a] Edward R. T. Tiekink[b] and Anton V. Dolzhenko*[ac]

Received 5th June 2020
Accepted 28th June 2020

DOI: 10.1039/d0ra04970k

rsc.li/rsc-advances

New 6,N^2-diaryl-1,3,5-triazine-2,4-diamines were designed using the 3D-QSAR model developed earlier. These compounds were prepared and their antiproliferative activity was evaluated against three breast cancer cell lines (MDA-MB231, SKBR-3 and MCF-7) and non-cancerous MCF-10A epithelial breast cells. The synthesized compounds demonstrated selective antiproliferative activity against triple negative MDA-MB231 breast cancer cells. The most active compound in the series inhibited MDA-MB231 breast cancer cell growth with a GI_{50} value of 1 nM. None of the tested compounds significantly affected the growth of the normal breast cells. The time-dependent cytotoxic effect, observed when cytotoxicity was assessed at different time intervals after the treatment, and morphological features, observed in the fluorescence microscopy and live cell imaging experiments, suggested apoptosis as the main pathway for the antiproliferative activity of these compounds against MDA-MB231 cells.

1. Introduction

Despite significant advancements in cancer therapy, cancer remains one of the diseases having the most negative impact on society. According to the World Health Organization, cancer was the second leading cause of patient lethality in 2018 causing almost 10 million deaths.[1] Moreover, the cancer prevalence and mortality from cancer have been continuously growing worldwide, in both developing and developed countries. It was projected that from 14 million people suffering from cancer in 2012 the number of new cases per year will double by 2030.

Breast cancer had the highest incidence rates among all types of cancer in 2018 (46.3 per 100 000 females). In females, breast cancer is the most frequently diagnosed type of cancer and the prevalent cause of cancer deaths.[1] Breast cancer is a rather heterogeneous form of cancer with cancer cells significantly varying in their properties and thus requiring different therapeutic approaches.[2] On the basis of presence or absence of molecular markers, breast cancer is classified into 4 main subtypes: (1) human epidermal growth factor 2 (ERBB2) positive cancer with cells expressing ERBB2, (2) luminal A breast cancer with cells expressing estrogen or progesterone receptors but not ERBB2, (3) luminal B breast cancer with cells expressing hormone receptors and ERBB2 negative cells, and (4) triple negative breast cancer with cells lacking molecular markers used for this classification.

The current therapeutic options and agents under development for the treatment of different types of breast cancer vary significantly. The cancer cells overexpressing hormone receptors can be targeted by anti-estrogenic medicines, like tamoxifen, by aromatase inhibitors, like letrozole, or other medicines for endocrine therapy. To improve therapeutic outcome of the endocrine therapy, other agents with different mechanisms have been investigated: pan-class I phosphatidylinositol 3-kinase (PI3K) inhibitors (*e.g.* alpelisib and buparlisib),[3,4] mammalian target of rapamycin (mTOR) inhibitors (*e.g.* everolimus),[5,6] and cyclin-dependent kinase CDK4 and CDK6 inhibitors (*e.g.* palbociclib and ribociclib).[7–9] For the treatment of ERBB2-positive breast cancer, PI3K and mTOR inhibitors are used together with ERBB2-targeted antibodies. Due to the absence of any targeted therapy for triple negative breast cancer, the general chemotherapy remains the main option available

[a]*School of Pharmacy, Monash University Malaysia, Jalan Lagoon Selatan, Bandar Sunway, Selangor Darul Ehsan 47500, Malaysia. E-mail: anton.dolzhenko@monash.edu*

[b]*Research Centre for Crystalline Materials, School of Science and Technology, Sunway University, 5 Jalan Universiti, Bandar Sunway, Selangor Darul Ehsan 47500, Malaysia*

[c]*School of Pharmacy and Biomedical Sciences, Curtin Health Innovation Research Institute, Faculty of Health Sciences, Curtin University, GPO Box U1987, Perth, Western Australia 6845, Australia*

† Electronic supplementary information (ESI) available: Copies of ^1H and ^{13}C NMR spectra of prepared compounds **1–21**; details of crystallographic study for compound **20**, plots of concentration–response curves for cytotoxicity experiments, video of live cell imaging of MDA-MB231 cells treated with compound **18**. CCDC 1934496. For ESI and crystallographic data in CIF or other electronic format see DOI: 10.1039/d0ra04970k

for the treatment of this most aggressive and mortal subtype of breast cancer. Typical medicines used against triple negative breast cancer include platinum drugs, taxanes, and anthracycline.[10] A group of promising emerging medicines, poly(ADP-ribose) polymerase inhibitors (*e.g.* olaparib and talazoparib), have been identified as a more specific therapy for a subgroup of triple negative breast cancer with cells having a mutation of BRCA1/BRCA2 genes.[11] New effective and selective anticancer agents are urgently needed for the safer and more effective treatment of triple negative breast cancer. The search for new potent compounds targeting breast cancer broadly covers various types of chemical structures.[12–14]

1,3,5-Triazine ring has been effectively used as a skeleton for the construction of new anticancer agents.[15] Recently, we identified 6,N^2-diaryl-1,3,5-triazine-2,4-diamines selectively targeting triple negative MDA-MB231 breast cancer cells.[16] We also developed a 3D-QSAR model for the prediction of antiproliferative activity of this type of compounds against MDA-MB231 breast cancer cells. Herein, we are testing predictive power of this model for the design of new anticancer agents with the 6,N^2-diaryl-1,3,5-triazine-2,4-diamine scaffold and continue our efforts on the development of highly potent and selective anticancer agents.

2. Results and discussion

2.1. QSAR-guided design of compounds

We previously reported synthesis of 6,N^2-substituted 1,3,5-triazine-2,4-diamines (126 compounds) and their cytotoxic activity against breast cancer cell lines (MDA-MB231, SKBR-3 and MCF-7) and non-cancerous epithelial breast cells (MCF-10A).[16] Some of the prepared compounds demonstrated selective activity against triple negative breast cancer cells (MDA-MB231). Twenty-five most active compounds were further evaluated and their GI_{50} values were estimated and used for the development of a 3D-QSAR model suitable for the design of new potent anticancer agents.[16] The model is based on the activity of compounds with different substituents in phenyl rings A and B (Fig. 1).

The developed 3D-QSAR model indicated that bulky electron donating groups at the phenyl in the position 6 of the triazine, *i.e.* ring A would improve antiproliferative activity of compounds against MDA-MB231 cells. Based on this model, we designed a group of compounds bearing suitable functional groups at the phenyl rings A and B, with an expectation of higher activity against triple negative breast cancer, and applied the model to predict pGI_{50} values for these compounds (Table 1).

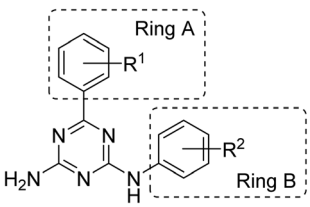

Fig. 1 General structure of the designed compounds.

Table 1 6,N^2-Diaryl-1,3,5-triazine-2,4-diamines (**1–21**) and their antiproliferative activity against MDA-MB231 cells predicted using the QSAR model developed earlier[16]

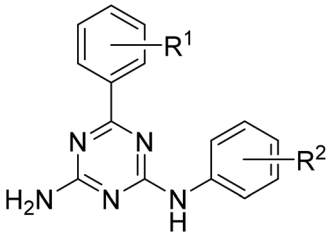

Compound	R^1	R^2	Predicted pGI_{50}
1	3-F	2-MeO	5.54
2	4-Cl	4-Me	5.51
3	4-CF_3	2-Cl	5.22
4	4-CF_3O	4-Cl	4.95
5	4-Me_2N	2-Cl	5.79
6	4-Me	2-Cl	5.65
7	4-Me	4-Cl	5.51
8	4-MeO	H	6.58
9	4-MeO	4-Me	5.41
10	3,4,5-$(MeO)_3$	H	5.58
11	3,4,5-$(MeO)_3$	2-F	4.85
12	3,4,5-$(MeO)_3$	2-Cl	5.10
13	3,4,5-$(MeO)_3$	2-MeO	4.78
14	3,4,5-$(MeO)_3$	3-Cl	4.62
15	3,4,5-$(MeO)_3$	3-Me	4.49
16	3,4,5-$(MeO)_3$	4-Cl	4.95
17	3,4,5-$(MeO)_3$	4-Br	4.45
18	3,4,5-$(MeO)_3$	4-Me	4.40
19	3,4,5-$(MeO)_3$	4-MeO	4.79
20	3,4,5-$(MeO)_3$	4-CF_3O	4.49
21	3,4,5-$(MeO)_3$	4-iPr	5.01

To test the earlier developed model, two main groups of compounds were selected for the synthesis. Number of substituents in each of the phenyl rings A and B for the first group of compounds (**1–9**) was limited to one functional group. The second group included 3,4,5-trimethoxyphenyl substituted compounds **10–21** to test effect of multiple substituents in ring A on the activity. Previously, we noticed that compounds with the R^1 group in *meta*-position of ring A retained activity with a greater variety of substituents at another phenyl ring. Contrary, activity of compounds with *para*-position of R^1 was very sensitive to the type and position of R^2, disappearing when R^2 was located in the *para*-position of ring B. Selecting compounds **10–21** with the preferred methoxy groups located in positions equivalent to the *para*- and both *meta*-positions of ring A, we intended to test which activity pattern they will follow. The predicted pGI_{50} values obtained from the 3D-QSAR model justified synthesis of the compounds.

2.2. Synthesis

Microwave irradiation has been widely used to facilitate synthesis of 1,3,5-triazines.[17] Sometimes, microwave irradiation

also changes outcome of reactions. The one-pot reaction of cyanoguanidine, benzaldehydes, and anilines in ethanol in the presence hydrochloric acid under conventional heating, followed by the treatment with aqueous sodium hydroxide (excess) was reported to produce 6,N^2-diaryl-5,6-dihydro-1,3,5-triazine-2,4-diamines.[18] However, a similar reaction under focused microwave irradiation resulted in the formation their fully aromatic analogues.[19] This microwave-assisted methodology we applied for synthesis of new 6,N^2-diaryl-1,3,5-triazine-2,4-diamines (**1–21**), which were designed using the 3D-QSAR model as describe above.

The reactions were performed in a one-pot manner with the three-component condensation of cyanoguanidine, benzaldehydes, and anilines at the first stage and the rearrangement accompanied with dehydrogenative aromatization at the second one (Scheme 1). The structure of the resulting 6,N^2-diaryl-1,3,5-triazine-2,4-diamines (**1–21**) was confirmed by the NMR spectroscopic data and X-ray crystallographic study on one representative product, compound **20**. The three diagnostic signals of the aromatic triazine ring quaternary carbon atoms appear in ^{13}C NMR spectra of **1–21** in the region 164.4–170.2 ppm. In the ^{1}H NMR spectra, the downfield shift of signals for protons in the *ortho*-positions of the phenyl ring directly attached to the 1,3,5-triazine ring should be attributed to the anisotropic effect of the coplanar triazine π-electron system.

X-ray crystallography of **20** (Fig. 2) showed that to a first approximation the molecule is planar and has the shape of the letter U as both appended aromatic rings are orientated to the same side of the molecule. Within the triazine ring, the near

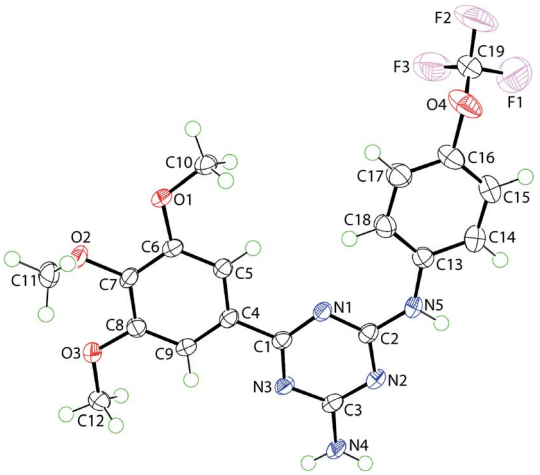

Fig. 2 Molecular structure of **20**, showing atom labelling scheme and anisotropic displacement parameters at the 70% probability level.

equivalence of the C–N bond lengths is indicative of substantial delocalisation of π-electron density over the ring. Details of crystallographic analysis are available in ESI.†

2.3. Biological evaluation

2.3.1. Cytotoxicity evaluation. The prepared compounds **1–21** were tested against three breast tumor cell lines: hormone (estrogen and progesterone) negative MDA-MB231 and hormone positive SKBR-3 and MCF-7. The initial screening of 6,N^2-diaryl-1,3,5-triazine-2,4-diamines (**1–21**) was performed at

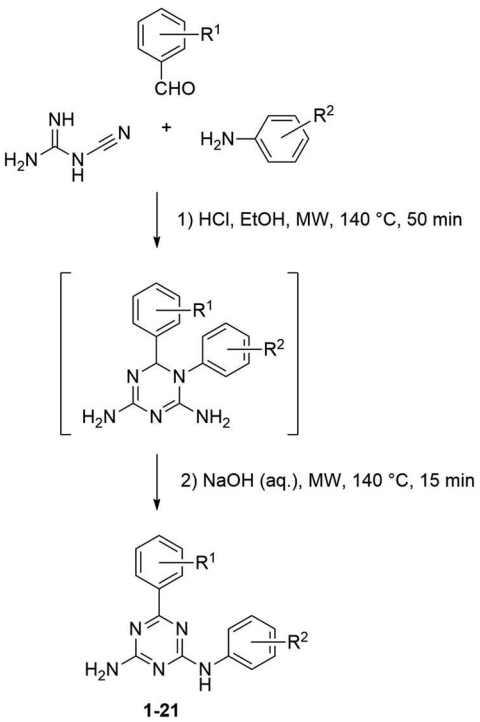

Compd.	R^1	R^2
1	3-F	2-MeO
2	4-Cl	4-Me
3	4-CF_3	2-Cl
4	4-CF_3O	4-Cl
5	4-Me_2N	2-Cl
6	4-Me	2-Cl
7	4-Me	4-Cl
8	4-MeO	H
9	4-MeO	4-Me
10	3,4,5-$(MeO)_3$	H
11	3,4,5-$(MeO)_3$	2-F
12	3,4,5-$(MeO)_3$	2-Cl
13	3,4,5-$(MeO)_3$	2-MeO
14	3,4,5-$(MeO)_3$	3-Cl
15	3,4,5-$(MeO)_3$	3-Me
16	3,4,5-$(MeO)_3$	4-Cl
17	3,4,5-$(MeO)_3$	4-Br
18	3,4,5-$(MeO)_3$	4-Me
19	3,4,5-$(MeO)_3$	4-MeO
20	3,4,5-$(MeO)_3$	4-CF_3O
21	3,4,5-$(MeO)_3$	4-*i*Pr

Scheme 1 Synthesis of 6,N^2-diaryl-1,3,5-triazine-2,4-diamines (**1–21**).

Table 2 Preliminary cytotoxic screening of 6,N^2-1,3,5-triazine-2,4-diamines (**1–21**) on breast cancer cell lines at 10 μM

Compound	R^1	R^2	Cell viability[a] (%)		
			MDA-MB231	SKBR-3	MCF-7
1	3-F	2-MeO	49	84	88
2	4-Cl	4-Me	29	85	100
3	4-CF_3	2-Cl	49	83	96
4	4-CF_3O	4-Cl	34	86	95
5	4-Me_2N	2-Cl	28	55	86
6	4-Me	2-Cl	36	80	51
7	4-Me	4-Cl	51	76	95
8	4-MeO	H	28	67	85
9	4-MeO	4-Me	32	89	99
10	3,4,5-$(MeO)_3$	H	14	37	62
11	3,4,5-$(MeO)_3$	2-F	34	73	98
12	3,4,5-$(MeO)_3$	2-Cl	42	80	100
13	3,4,5-$(MeO)_3$	2-MeO	16	57	100
14	3,4,5-$(MeO)_3$	3-Cl	40	58	96
15	3,4,5-$(MeO)_3$	3-Me	14	43	86
16	3,4,5-$(MeO)_3$	4-Cl	20	48	52
17	3,4,5-$(MeO)_3$	4-Br	24	43	48
18	3,4,5-$(MeO)_3$	4-Me	14	37	62
19	3,4,5-$(MeO)_3$	4-MeO	20	48	52
20	3,4,5-$(MeO)_3$	4-CF_3O	20	45	51
21	3,4,5-$(MeO)_3$	4-iPr	9	42	49

[a] MTT method, cells incubated with corresponding compounds (10 μM) for 72 h. Values are mean of three independent experiments.

one point concentration (10 μM) for preliminary assessment of their antiproliferative potential (Table 2). Percentage cell viability was calculated 72 h after treatment with compounds. In general, triple negative breast cancer cells (MDA-MB231) were more responsive than hormone positive breast cancer cells (SKBR-3 and MCF-7) to the treatment with the compounds. These results are similar to the trend observed earlier for their structural analogues.[16]

Since all compounds **1–21** demonstrated significant antiproliferative activity against MDA-MB231 cells at the screening concentration, they were further tested at concentration ranging from 0.00002 μM to 20 μM to estimate their 50% growth inhibitory concentrations (GI_{50}) against breast cancer cells (Table 3). Nilotinib and methotrexate were used as positive controls. For compounds active at the screening concentration against SKBR-3 and MCF-7 cells, concentration-dependent response was also evaluated and the corresponding GI_{50} values were estimated.

Compounds **1–21** were also tested against MCF-10A normal breast cells to evaluate their selectivity towards cancer cells. None of the compounds showed significant inhibition of the normal breast cell growth at the compound concentration of 20 μM.

The prepared 6,N^2-diaryl-1,3,5-triazine-2,4-diamines **1–21** possessed specific cytotoxicity against triple negative MDA-MB231 breast cancer cells with GI_{50} values ranging widely. However, the most intriguing results were obtained for compounds **10–21** with the 3,4,5-trimethoxyphenyl moiety as the ring A. This substitution was exceptionally beneficial for the anticancer activity, particularly in a combination with the *para*-substitution at the phenyl ring B. Changing location of the substituents to *ortho*- or *meta*-position in the phenylamino moiety dramatically decreased potency of compounds. The GI_{50} values for these subgroups have a 2–3 order difference. For example, relocation of the methoxy group from the *ortho*- to *para*-position of the ring B resulted in a 200-fold increase in the antiproliferative activity (**13** *vs.* **19**). Even greater improvement in the activity was achieved when methyl or chloro substituents changed their location at the ring B from *meta*- to *para*-position leading to compounds 1300–2000-fold more potent than their regioisomers (**14** *vs.* **16**, **15** *vs.* **18**). At the same time, it appeared that for the trimethoxyphenyl-substituted series (**10–21**) an increase in size of the R^2 group in *para*-position from the most potent compound with a methyl group (**18**) decreased the activity. Nevertheless, most of the triazines combining trimethoxyphenyl as the ring A and *para*-substituted phenylamino moieties as the ring B possessed activity comparable or higher than that of reference drugs methotrexate and nilotinib. These compounds also demonstrated good antiproliferative activity against SKBR-3 cells. The most active 6,N^2-diaryl-1,3,5-triazine-2,4-diamine identified in the series was compound **18**, which was 10-fold more active than methotrexate and 40-fold more potent than nilotinib against MDA-MB231 breast cancer cells. This compound (**18**) and its analogue **16**, with the chloro substituent instead of the *para*-methyl group in the ring B, were selected for further experiments to better understand processes underlying antiproliferative effects of these compounds.

To assess predictive power of the earlier developed 3D-QSAR model, we compared experimental and predicted pGI_{50} values, calculated using the 3D-QSAR model (Table 4). The residual error values for the first series of compounds (**1–9**) were rather acceptable *viz.* without extreme differences between the experimental and predicted values. However, a large discrepancy between the predicted and experimental values was observed for many trimethoxyphenyl-substituted compounds. These compounds, especially those with the R^2 group in *para*-position of the ring B (**16–21**), appeared to be much more potent than it was predicted by the model. These findings indicated a limitation of the earlier prepared 3D-QSAR model,[16] which seemed to be valid for compounds with monosubstituted phenyl rings and should be used with a caution for more complex structures.

2.3.2. Time-dependent cytotoxicity. To further evaluate cytotoxicity of the prepared compound against cancer cells, time-dependent cell viability experiments were carried out with the selected most active compounds **16** and **18** using MDA-MB231 breast cancer cell line. The MDA-MB231 cell viability was assessed after the exposure of the cells to compounds **16** or **18** for 12, 24, 48, and 72 h at concentrations ranging from 0.2 nM to 125 nM. The GI_{50} values were estimated when treatment with the highest concentration (125 nM) of tested compounds resulted in more than 80% of cell growth inhibition (Table 5).

Compound **18** possessed higher antiproliferative activity than **16** against MDA-MB231 cells for all duration of observations. For both compounds, the cytotoxic effect developed gradually and no significant inhibition of the cell growth was

Table 3 Cytotoxicity[a] of 6,N^2-diaryl-1,3,5-triazine-2,4-diamines (**1–21**)

			$GI_{50} \pm SD$[b] (μM)			
Compound	R^1	R^2	MDA-MB231	SKBR-3	MCF-7	MCF-10A
1	3-F	2-MeO	17.3 ± 0.6	>20	>20	>20
2	4-Cl	4-Me	13.8 ± 1.9	>20	>20	>20
3	4-CF_3	2-Cl	13.7 ± 0.6	17.7 ± 1.4	>20	>20
4	4-CF_3O	4-Cl	16.7 ± 1.2	>20	>20	>20
5	4-Me_2N	2-Cl	0.1 ± 0.001	0.4 ± 0.04	>20	>20
6	4-Me	2-Cl	3.8 ± 0.4	>20	10.7 ± 1.0	>20
7	4-Me	4-Cl	9.6 ± 0.2	>20	>20	>20
8	4-MeO	H	8.4 ± 0.3	19.6 ± 0.9	14.2 ± 1.7	>20
9	4-MeO	4-Me	6.1 ± 0.6	>20	>20	>20
10	3,4,5-$(MeO)_3$	H	9.7 ± 0.6	17.2 ± 0.4	>20	>20
11	3,4,5-$(MeO)_3$	2-F	7.9 ± 0.5	>20	>20	>20
12	3,4,5-$(MeO)_3$	2-Cl	11.3 ± 1.1	>20	>20	>20
13	3,4,5-$(MeO)_3$	2-MeO	2.1 ± 0.2	14.0 ± 1.6	>20	>20
14	3,4,5-$(MeO)_3$	3-Cl	9.1 ± 1.1	16.7 ± 1.4	>20	>20
15	3,4,5-$(MeO)_3$	3-Me	2.2 ± 0.2	6.0 ± 0.1	>20	>20
16	3,4,5-$(MeO)_3$	4-Cl	0.007 ± 0.00001	0.3 ± 0.04	12.5 ± 0.2	>20
17	3,4,5-$(MeO)_3$	4-Br	0.008 ± 0.0005	0.17 ± 0.01	>20	>20
18	3,4,5-$(MeO)_3$	4-Me	0.001 ± 0.00001	0.21 ± 0.01	>20	>20
19	3,4,5-$(MeO)_3$	4-MeO	0.01 ± 0.001	0.27 ± 0.02	>20	>20
20	3,4,5-$(MeO)_3$	4-CF_3O	1.5 ± 0.1	5.0 ± 0.35	>20	>20
21	3,4,5-$(MeO)_3$	4-iPr	0.04 ± 0.002	1.1 ± 0.05	10.7 ± 1.1	>20
Methotrexate[c]			0.01 ± 0.001	ND	5.8 ± 0.5	ND
Nilotinib[c]			0.04 ± 0.001	9.60 ± 0.5	ND	ND

[a] MTT method, cells incubated with compounds for 72 h, experiments performed in triplicates. [b] Standard deviation of mean values. [c] Positive control.

detected 12 h after the treatment. However, compound **18** started showing activity in nanomolar concentrations (GI_{50} = 5 nM) at 24 h with an increase in the potency over the following 24 h (GI_{50} = 4 nM) and even more after the total exposure for 72 h (GI_{50} = 1 nM). A similar time-dependent pattern was observed for compound **16**.

Table 4 Antiproliferative activities obtained experimentally and predicted for 6,N^2-diaryl-1,3,5-triazine-2,4-diamines (**1–21**) by the 3D-QSAR model[a]

Compound	R^1	R^2	Experimental pGI_{50}[b]	Predicted pGI_{50}[c]	Residual error[d]
1	3-F	2-MeO	4.76	5.54	−0.78
2	4-Cl	4-Me	4.86	5.51	−0.64
3	4-CF_3	2-Cl	4.86	5.22	−0.35
4	4-CF_3O	4-Cl	4.78	4.95	−0.18
5	4-Me_2N	2-Cl	7.00	5.79	1.21
6	4-Me	2-Cl	5.42	5.65	−0.23
7	4-Me	4-Cl	5.02	5.51	−0.49
8	4-MeO	H	5.08	6.58	−1.50
9	4-MeO	4-Me	5.21	5.41	−0.19
10	3,4,5-$(MeO)_3$	H	5.01	5.58	−0.56
11	3,4,5-$(MeO)_3$	2-F	5.10	4.85	0.25
12	3,4,5-$(MeO)_3$	2-Cl	4.95	5.10	−0.15
13	3,4,5-$(MeO)_3$	2-MeO	5.69	4.78	0.91
14	3,4,5-$(MeO)_3$	3-Cl	5.04	4.62	0.42
15	3,4,5-$(MeO)_3$	3-Me	5.66	4.49	1.17
16	3,4,5-$(MeO)_3$	4-Cl	8.15	4.95	3.20
17	3,4,5-$(MeO)_3$	4-Br	8.10	4.45	3.65
18	3,4,5-$(MeO)_3$	4-Me	8.70	4.40	4.30
19	3,4,5-$(MeO)_3$	4-MeO	8.00	4.79	3.21
20	3,4,5-$(MeO)_3$	4-CF_3O	5.83	4.49	1.34
21	3,4,5-$(MeO)_3$	4-iPr	7.40	5.01	2.39

[a] QSAR model reported earlier.[16] [b] Experimental pGI_{50} calculated as $pGI_{50} = -\log 10 \times GI_{50}$. [c] pGI_{50} values predicted by the QSAR model. [d] Difference between the predicted and experimental pGI_{50} values.

Table 5 Time-dependent cytotoxic effect[a] of the most active compounds (16 and 18) against MDA-MB231 breast cancer cell line

	$GI_{50} \pm SD$ (nM) or growth inhibition at 125 nM			
Compound	12 h	24 h	48 h	72 h
16	17%[b]	61%[b]	75%[b]	7 ± 0.6
18	15%[b]	5 ± 0.1	4 ± 0.3	1 ± 0.02

[a] MTT method, values are the mean ± SD, all experiments performed at least three times. [b] Percentage cell growth inhibition at 125 nM concentration of test compounds.

These results suggest that the antiproliferative effect of compounds **16** and **18** develop gradually and without an immediate toxic effect on the cells. A negligible cytotoxicity 12 h after the treatment suggests that the compounds are less likely to cause cell necrosis and probably induce apoptosis. To further test this assumption, we performed fluorescent microscopy experiments assessing effects of compounds **16** and **18** on the morphology of MDA-MB231 breast cancer cell.

2.3.3. Acridine orange and propidium iodide double staining experiments. After the determination of cytotoxicity by the MTT assay, morphological changes of MDA-MB231 cells treated with most active compounds **16** and **18** were studied using fluorescence microscopy. The acridine orange (AO) and propidium iodide (PI) double staining method was used to determine morphological features of apoptotic cells (chromatin condensation, cell blebbing and apoptotic bodies). AO emits green light by intercalating the DNA of the live and dead cells, while PI emits red fluorescence by intercalating the DNA of dead cells only.[20]

MDA-MB231 cells were treated with compounds **16** and **18** and incubated for 24 h prior to the observation of changes in cell morphology. The selected representative images of fluorescence microscopy are presented in Fig. 3: live cells emit green color (white arrow) because of AO intercalation with DNA and apoptotic cells appear reddish-orange (red arrow) by intercalating PI to the DNA because of altered membrane permeability. Mid-stage apoptosis is evident by the presence of cells with nuclear chromatic condensation (blue arrow), cell blebbing (purple arrow), and multi-nucleated cells (yellow arrow).

2.3.4. Live cell imaging. To visualize morphological changes in the cells in real time, live cell imaging of MDA-MB231 cells treated with compound **18** was carried out. The cells were stained with AO and PI and treated with **18** (10 μM). The pictures were taken after every 10 minutes for 4 h and intercalated into video (see ESI†). The video clearly shows the morphological changes of the cells initiated by **18** at different times, like formation of multinucleation, chromatin condensation, cell blebbing and apoptotic bodies. The death of the breast cancer cells (MDA-MB231) treated with compound **18** was also evident from turning of live cells (green color) to dead cells (red color). These observations suggest that compound **18** realizes its cytotoxic activity by inducing apoptosis in MDA-MB231 cells.

2.4. Prediction of ADME properties

In the design of biologically active agents, optimization of lead compounds and selection of drug candidates, *in silico* evaluation of absorption, distribution, metabolism and elimination (ADME) of compounds has become a common practice.[21]

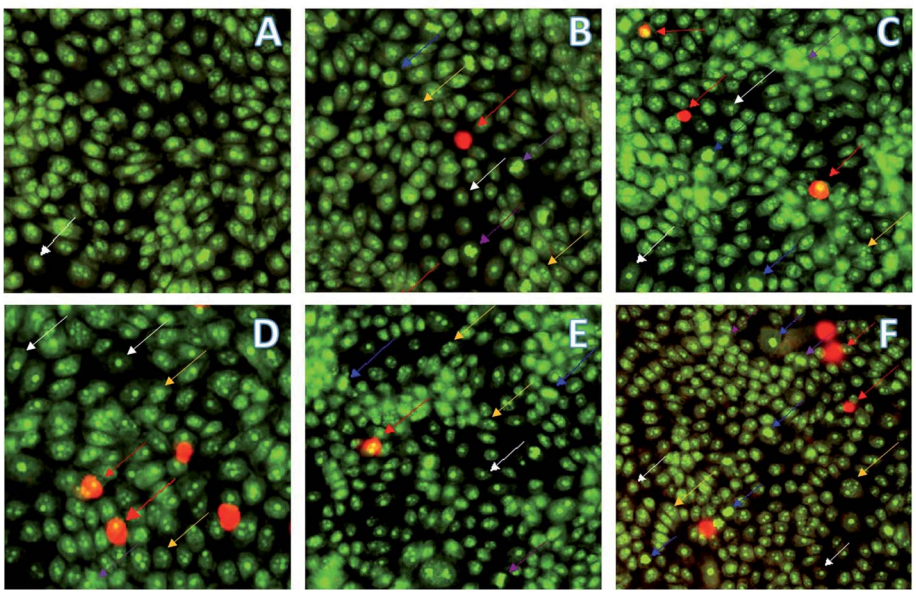

Fig. 3 AO/PI double staining of MDA-MB231 cells with signs of apoptosis 24 h after the treatment with compounds. (A) Cells treated with a vehicle, 1% DMSO, negative control; (B) cells treated with compound **16** (125 nM); (C) cells treated with compound **16** with (250 nM); (D) cells treated with methotrexate (10 nM), positive control; (E) cells treated with compound **18** IC_{20} (2.5 nM); (F) cells treated with compound **18** IC_{50} (5 nM). Images were taken with a fluorescence microscope at 400×. White arrow points to live cells, red arrow shows apoptotic cells, blue arrow points to chromatin condensation, purple arrow shows cell blebbing and yellow arrow indicates multi-nucleated cells.

Table 6 Selected ADME properties of 6,N^2-diaryl-1,3,5-triaizne-2,4-diamines (**1–21**)[a]

Compound	MW[b]	SASA[c]	Donor HB[d]	Accpt HB[e]	*QP* log *P* o/w[f]	*QPP* Caco[g]	#Metab[h]	Percent human oral absorption[i]
1	311.32	663.94	3	4.75	3.50	849.24	2	100
2	311.77	659.67	3	4.00	3.86	784.19	1	100
3	365.75	642.85	3	4.00	4.06	922.41	1	100
4	381.74	696.37	3	4.00	4.56	800.65	1	100
5	340.81	709.92	3	5.00	4.03	903.51	2	100
6	311.77	664.90	3	4.00	3.89	924.51	2	100
7	311.77	668.19	3	4.00	3.87	783.98	1	100
8	293.33	644.11	3	4.75	3.17	789.12	2	100
9	307.35	666.66	3	4.75	3.44	787.51	2	100
10	353.38	735.08	3	6.25	3.43	825.33	4	100
11	371.37	742.37	3	6.25	3.67	887.43	4	100
12	387.83	755.90	3	6.25	3.93	969.42	4	100
13	383.41	766.44	3	7.00	3.34	893.13	5	100
14	387.83	759.21	3	6.25	3.91	822.03	4	100
15	367.41	766.57	3	6.25	3.72	824.23	5	100
16	387.83	759.20	3	6.25	3.91	822.03	3	100
17	432.28	764.15	3	6.25	3.99	821.52	3	100
18	367.41	758.05	3	6.25	3.71	822.74	4	100
19	383.41	750.27	3	7.00	3.44	821.39	4	100
20	437.38	803.46	3	6.25	4.78	802.60	4	100
21	395.46	800.44	3	6.25	4.27	818.46	4	100

[a] Calculated using QikProp 4.3 module of the Schrödinger software. [b] Molecular weight. [c] Total solvent accessible surface area in Å^2 using a probe with a 1.4 Å radius, range 95% of drugs (300.0–1000.0). [d] Estimated number of hydrogen bonds that would be donated by the solute to water molecules in an aqueous solution, range 95% of drugs (0.0–6.0). [e] Estimated number of hydrogen bonds that would be accepted by the solute from water molecules in an aqueous solution, range 95% of drugs (2.0–20.0). [f] Predicted log of the octanol/water partition coefficient, range 95% of drugs (−2–6.5). [g] Caco-2 cell permeability in nm s^{-1}, range 95% of drugs (<25 poor, >500 great). Caco-2 cells are a model for the gut blood barrier, non-active transport. [h] Number of likely metabolic reactions; range 95% of drugs (1–8). [i] Human oral absorption predicted on the basis of a quantitative multiple linear regression model. 0 to 100% scale (>85% high).

QikProp (version 4.3) module of the Schrödinger software was used to predict the molecular properties influencing critical pharmacokinetic parameters of compounds **1–21** (Table 6). Parameters like octanol/water partition coefficient (*QP* log *P*, o/w) and aqueous solubility (*QP* log *S*) are important for the prediction of drug absorption, transport and distribution in the body. These parameters calculated for **1–12** have values similar to those, which are typical for commonly used drugs. Steric and molecular surface descriptors *i.e.*, total solvent accessible area (SASA) and its hydrophobic (FOSA) and hydrophilic (FISA) components were also calculated and found to be within the 95% range of values for known drugs. Lipinski's rule of five has been often used as a first filter for the prediction the drug-like properties of compounds.[22] None of the prepared compounds violate Lipinski's rule of five. The complete absorption and absence of effects on CNS were predicted for compounds **1–21**. Overall, all evaluated compounds were predicted to possess ADME properties favorable for potential agents targeting breast cancer cells. More detailed ADME profile for the compounds predicted by QikProp module is available in ESI.†

3. Conclusions

We synthesized a library of novel 6,N^2-diaryl-1,3,5-triazine-2,4-diamines designed using the 3D-QSAR data from the previous report.[16] Their antiproliferative activity was evaluated against three breast cancer cell lines and it was found that triple negative breast cancer cells (MDA-MB231) were significantly more sensitive to the treatment with the prepared compounds. Some 6,N^2-diaryl-1,3,5-triazine-2,4-diamines demonstrated good antiproliferative activity against SKBR-3 cells, but MCF-7 cells were generally resistant to the treatments with these compounds.

Some of the synthesized compounds demonstrated even greater activity against MDA-MB231 cells than it was predicted by the 3D-QSAR model. The 3D-QSAR model limitation might originate from multiple targets responsible for the activity of 6,N^2-diaryl-1,3,5-triazine-2,4-diamines and hence requires further investigations. The discrepancy between the predicted values and the experimental data was particularly evident for N^2-aryl-6-(3,4,5-trimethoxyphenyl)-1,3,5-triazine-2,4-diamines **16–21** possessing *para*-substituted phenyl ring B. The most active compound in the series also belongs to this group: compound **18** inhibited triple negative MDA-MB231 breast cancer cell growth with GI_{50} value of 1 nM. Importantly, the prepared compounds demonstrated no cytotoxicity towards non-cancerous MCF-10A breast cells. The cytotoxic evaluation at different time intervals for the most active compounds **16** and **18** showed that these compounds possessed a concentration- and time-dependent cytotoxic effect on MDA-MB231 breast cancer cells. Morphological features observed by the fluorescent microscopy and live cell imaging after the AO/PI double staining

suggested that the tested compounds induced apoptosis in MDA-MB231 cells. All compounds, including **18**, were predicted to have ADME profiles favorable for potential antiproliferative agents targeting breast cancer.

4. Experimental

4.1. General

Melting points (uncorrected) were determined using a Stuart™ SMP40 automatic melting point apparatus. ^{1}H and ^{13}C NMR spectra were recorded on a Bruker Fourier NMR spectrometer (300 MHz) using DMSO-d_6 as a solvent and TMS as an internal reference. Microwave-assisted reactions were carried out in the closed vessel focused single mode using a Discover SP microwave synthesizer (CEM, USA) monitoring reaction temperature by the equipped IR sensor.

4.2. General method for the synthesis of 6,N^2-diaryl-1,3,5-triazine-2,4-diamines (1–21)

The microwave irradiation parameters optimized earlier[19] for the synthesis of 6,N^2-diaryl-1,3,5-triazine-2,4-diamines were applied for the preparation of **1–21**. To a solution of cyanoguanidine (0.21 g, 2.5 mmol), a substituted benzaldehyde (2.5 mmol), and an aniline (2.5 mmol) in EtOH (2 mL) in a 10 mL seamless pressure vial, conc. HCl (0.21 mL, 2.5 mmol) was added. The reaction mixture was heated at 140 °C for 50 min by irradiation in the Discover SP (CEM) microwave reactor operating at maximal microwave power up to 150 W. Then, an aq. solution of NaOH (5 N, 1 mL) was added to the reaction mixture and heating was continued for another 15 min at 140 °C. After cooling, the precipitated product was filtered, washed with water and recrystallized from suitable solvents (EtOH, aq. EtOH, or MeCN) specified below. Yields of products **1–21** are reported as overall isolated yields for the one-pot procedure.

4.2.1. 6-(3-Fluorophenyl)-N^2-(2-methoxyphenyl)-1,3,5-triazine-2,4-diamine (1). Yield 33%. Mp 140–142 °C (EtOH/water). ^{1}H NMR (300 MHz, DMSO-d_6): δ 3.87 (OCH_3), 6.95–7.10 (3H, m, H-3″, H-4″ and H-5″), 7.22 (2H, brs, NH_2), 7.40 (1H, dddd, $^4J_{HH}$ = 0.8 Hz, $^4J_{HH}$ = 2.6 Hz, $^3J_{HH}$ = 8.5 Hz, $^3J_{HF}$ = 8.4 Hz, H-4′), 7.56 (1H, ddd, $^4J_{HF}$ = 6.0 Hz, $^3J_{HH}$ = 8.0 Hz, $^3J_{HH}$ = 8.0 Hz, H-5′), 8.00 (1H, ddd, $^4J_{HH}$ = 1.3 Hz, $^4J_{HH}$ = 2.6 Hz, $^3J_{HF}$ = 10.6 Hz, H-2′), 8.12 (1H, s, NH), 8.13–8.17 (2H, m, H-6″ and H-6′); ^{13}C NMR (75 MHz, DMSO-d_6): δ 55.7 (OCH_3), 111.0 (C-3″), 114.0 (d, $^2J_{CF}$ = 23.1 Hz, C-2′), 118.2 (d, $^2J_{CF}$ = 21.8 Hz, C-4′), 120.2 (C-5″), 122.3 (C-6″), 123.7 (d, $^4J_{CF}$ = 2.2 Hz, C-6′), 123.8 (C-4″), 127.6 (C-1″), 130.3 (d, $^3J_{CF}$ = 8.2 Hz, C-5′), 139.2 (d, $^3J_{CF}$ = 7.5 Hz, C-1′), 149.9 (C-2″), 162.1 (d, $^1J_{CF}$ = 242.9 Hz, C-3′), 164.6 (C-2), 167.2 (C-4), 169.0 (d, $^4J_{CF}$ = 3.0 Hz, C-6). Anal. calcd for $C_{16}H_{14}FN_5O$: C, 61.73; H, 4.53; N, 22.50. Found: C, 61.65; H, 4.77; N, 22.26.

4.2.2. 6-(4-Chlorophenyl)-N^2-(4-methylphenyl)-1,3,5-triazine-2,4-diamine (2). Yield 45%. Mp 179–181 °C (MeCN). ^{1}H NMR (300 MHz, DMSO-d_6): δ 2.27 (3H, s, CH_3), 7.11 (2H, d, J = 8.3 Hz, H-3″ and H-5″), 7.12 (2H, brs, NH_2), 7.58 (2H, d, J = 8.6 Hz, H-3′ and H-5′), 7.68 (2H, d, J = 8.3 Hz, H-2″ and H-6″), 8.29 (2H, d, J = 8.6 Hz, H-2′ and H-6′), 9.46 (1H, s, NH); ^{13}C NMR (75 MHz, DMSO-d_6): δ 20.3 (CH_3), 120.1 (C-2″ and C-6″), 128.4 (C-3′ and C-5′), 128.8 (C-3″ and C-5″), 129.4 (C-2′ and C-6′), 130.9 (C-1″), 135.7 (C-1′), 136.1 (C-4′), 137.2 (C-4″), 164.5 (C-4), 167.1 (C-6), 169.1 (C-2). Anal. calcd for $C_{16}H_{14}ClN_5$: C, 61.64; H, 4.53; N, 22.46. Found: C, 61.54; H, 4.50; N, 22.29.

4.2.3. N^2-(2-Chlorophenyl)-6-(4-(trifluoromethyl)phenyl)-1,3,5-triazine-2,4-diamine (3). Yield 38%. Mp 165–167 °C (EtOH). ^{1}H NMR (300 MHz, DMSO-d_6): δ 7.23 (2H, brs, NH_2), 7.23 (1H, ddd, J = 1.6 Hz, J = 7.7 Hz, J = 7.7 Hz, H-4″), 7.38 (1H, ddd, J = 1.3 Hz, J = 7.7 Hz, J = 7.7 Hz, H-5″), 7.53 (1H, dd, J = 1.4 Hz, J = 8.0 Hz, H-3″), 7.80 (1H, dd, J = 1.6 Hz, J = 8.0 Hz, H-6″), 7.88 (2H, d, J = 8.3 Hz, H-3′ and H-5′), 8.45 (2H, d, J = 8.1 Hz, H-2′ and H-6′), 8.97 (1H, s, NH); ^{13}C NMR (75 MHz, DMSO-d_6): δ 120.5 (q, $^1J_{CF}$ = 273.6 Hz, CF_3), 125.2 (q, $^3J_{CF}$ = 3.5 Hz, C-3′ and C-5′), 126.2 (C-6″), 127.3 (C-2″), 127.5 (C-5″), 128.4 (C-2′ and C-6′), 128.5 (C-4″), 129.4 (C-3″), 131.1 (q, $^2J_{CF}$ = 31.8, C-4′), 135.6 (C-1″), 140.5 (C-1′), 165.3 (C-4), 167.3 (C-6), 169.0 (C-2). Anal. calcd for $C_{16}H_{11}ClF_3N_5$: C, 52.54; H, 3.03; N, 19.15. Found: C, 52.33; H, 2.95; N, 18.98.

4.2.4. N^2-(4-Chlorophenyl)-6-(4-(trifluoromethoxy)phenyl)-1,3,5-triazine-2,4-diamine (4). Yield 55%. Mp 201–203 °C (EtOH). ^{1}H NMR (300 MHz, DMSO-d_6): δ 7.27 (2H, brs, NH_2), 7.36 (2H, d, J = 8.9 Hz, H-3″ and H-5″), 7.51 (2H, dd, $^5J_{HF}$ = 0.9 Hz, $^3J_{HH}$ = 9.0 Hz, H-3′ and H-5′), 7.89 (2H, d, J = 8.9 Hz, H-2″ and H-6″), 8.43 (2H, d, J = 8.9 Hz, H-2′ and H-6′), 9.75 (1H, s, NH); ^{13}C NMR (75 MHz, DMSO-d_6): δ 120.0 (q, $^1J_{CF}$ = 257.0 Hz, OCF_3), 120.5 (C-3′ and C-5′), 121.4 (C-2″ and C-6″), 125.7 (C-1″), 128.2 (C-3″ and C-5″), 129.9 (C-2′ and C-6′), 135.7 (C-1′), 138.8 (C-4″), 150.6 (q, $^3J_{CF}$ = 1.7 Hz, C-4′), 164.5 (C-4), 167.1 (C-6), 169.1 (C-2). Anal. calcd for $C_{16}H_{11}ClF_3N_5O$: C, 50.34; H, 2.90; N, 18.35. Found: C, 50.22; H, 3.02; N, 18.26.

4.2.5. N^2-(2-Chlorophenyl)-6-(4-(dimethylamino)phenyl)-1,3,5-triazine-2,4-diamine (5). Yield 15%. Mp 191–193 °C (EtOH). ^{1}H NMR (300 MHz, DMSO-d_6): δ 2.99 (6H, s, $N(CH_3)_2$), 6.74 (2H, d, J = 9.1 Hz, H-3′ and H-5′), 6.89 (2H, brs, NH_2), 7.16 (1H, ddd, J = 1.6 Hz, J = 7.7 Hz, J = 7.7 Hz, H-4″), 7.36 (1H, ddd, J = 1.2 Hz, J = 7.8 Hz, J = 7.8 Hz, H-5″), 7.50 (1H, dd, J = 1.5 Hz, J = 8.0 Hz, H-3″), 7.96 (1H, dd, J = 1.5 Hz, J = 8.1 Hz, H-6″), 8.13 (2H, d, J = 9.2 Hz, H-2′ and H-6′), 8.43 (1H, s, NH); ^{13}C NMR (75 MHz, DMSO-d_6): δ 39.6 ($N(CH_3)_2$), 110.9 (C-3′ and C-5′), 123.2 (C-1′), 125.2 (C-6″), 126.2 (C-2″), 126.9 (C-4″), 127.2 (C-5″), 129.2 (C-2′ and C-6′), 129.2 (C-3″), 135.9 (C-1″), 152.5 (C-4′), 164.8 (C-4), 167.0 (C-6), 170.2 (C-2). Anal. calcd for $C_{17}H_{17}ClN_6$: C, 59.91; H, 5.03; N, 24.66. Found: C, 59.79; H, 4.96; N, 24.47.

4.2.6. N^2-(2-Chlorophenyl)-6-(4-methylphenyl)-1,3,5-triazine-2,4-diamine (6). Yield 40%. Mp 146–148 °C (EtOH). ^{1}H NMR (300 MHz, DMSO-d_6): δ 2.37 (3H, s, CH_3), 7.07 (2H, brs, NH_2), 7.20 (1H, ddd, J = 1.6 Hz, J = 7.8 Hz, J = 7.6 Hz, H-4″), 7.29 (2H, d, J = 8.0 Hz, H-3′ and H-5′), 7.37 (1H, ddd, J = 1.4 Hz, J = 7.7 Hz, J = 7.9 Hz, H-5″), 7.52 (1H, dd, J = 1.4 Hz, J = 8.0 Hz, H-3″), 7.87 (1H, dd, J = 1.5 Hz, J = 8.1 Hz, H-6″), 8.18 (2H, d, J = 8.2 Hz, H-2′ and H-6′), 8.71 (1H, s, NH); ^{13}C NMR (75 MHz, DMSO-d_6): δ 21.0 (CH_3), 125.7 (C-6″), 126.9 (C-4″), 127.2 (C-2″), 127.8 (C-5″, C-3′ and C-5′), 128.8 (C-2′ and C-6′), 129.3 (C-3″), 133.8 (C-1′), 135.7 (C-1″), 141.2 (C-4′), 165.1 (C-4), 167.2 (C-6), 170.2 (C-2). Anal. calcd for $C_{16}H_{14}ClN_5$: C, 61.64; H, 4.53; N, 22.46. Found: C, 61.53; H, 4.35; N, 22.28.

4.2.7. N^2-(4-Chlorophenyl)-6-(4-methylphenyl)-1,3,5-triazine-2,4-diamine (7). Yield 26%. Mp 202–204 °C (MeCN). ^{1}H NMR (300 MHz, DMSO-d_6): δ 2.08 (3H, s, CH_3), 7.14 (2H, brs, NH_2), 7.32 (2H, d, J = 8.6 Hz, H-3′ and H-5′), 7.35 (2H, d, J = 9.0 Hz, H-3″ and H-5″), 7.90 (2H, d, J = 8.9 Hz, H-2″ and H-6″), 8.23 (2H, d, J = 8.2 Hz, H-2′ and H-6′), 9.65 (1H, s, NH); ^{13}C NMR (75 MHz, DMSO-d_6): δ 21.0 (CH_3), 121.2 (C-2″ and C-6″), 125.4 (C-1″), 127.8 (C-3′ and C-5′), 128.2 (C-3″ and C-5″), 128.8 (C-2′ and C-6′), 133.9 (C-1′), 139.0 (C-4″), 141.3 (C-4′), 164.4 (C-4), 167.0 (C-6), 170.2 (C-2). Anal. calcd for $C_{16}H_{14}ClN_5$: C, 61.64; H, 4.53; N, 22.46. Found: C, 61.49; H, 4.47; N, 22.32.

4.2.8. 6-(4-Methoxyphenyl)-N^2-phenyl-1,3,5-triazine-2,4-diamine (8). Yield 50%. Mp 190–192 °C (EtOH). ^{1}H NMR (300 MHz, DMSO-d_6): δ 3.84 (3H, OCH_3), 7.00 (1H, t, J = 7.4 Hz, H-4″), 7.04 (2H, brs, NH_2), 7.07 (2H, d, J = 9.0 Hz, H-3′ and H-5′), 7.31 (2H, dd, J = 7.5 Hz, J = 8.4 Hz, H-3″ and H-5″), 7.86 (2H, dd, J = 1.1 Hz, J = 8.6 Hz H-2″ and H-6″), 8.31 (2H, d, J = 9.0 Hz, H-2′ and H-6′), 9.46 (1H, s, NH); ^{13}C NMR (75 MHz, DMSO-d_6): δ 55.2 (OCH_3), 113.6 (C-3′ and C-5′), 119.8 (C-2″ and C-6″), 121.8 (C-1″), 128.3 (C-3″ and C-5″), 129.0 (C-1′), 129.5 (C-2′ and C-6′), 140.0 (C-4″), 161.9 (C-4′), 164.5 (C-4), 167.0 (C-6), 169.8 (C-2). Anal. calcd for $C_{16}H_{15}N_5O$: C, 65.52; H, 5.15; N, 23.88. Found: C, 65.52; H, 5.15; N, 23.88.

4.2.9. 6-(4-Methoxyphenyl)-N^2-(4-methylphenyl)-1,3,5-triazine-2,4-diamine (9). Yield 41%. Mp 186–188 °C (MeCN). ^{1}H NMR (300 MHz, DMSO-d_6): δ 2.27 (3H, s, CH_3), 3.84 (3H, s, OCH_3), 6.99 (2H, brs, NH_2), 7.06 (2H, d, J = 9.0 Hz, H-3′ and H-5′), 7.11 (2H, d, J = 8.3 Hz, H-3″ and H-5″), 7.71 (2H, d, J = 8.4 Hz, H-2″ and H-6″), 8.29 (2H, d, J = 9.0 Hz, H-2′ and H-6′), 9.35 (1H, s, NH); ^{13}C NMR (75 MHz, DMSO-d_6): δ 20.3 (CH_3), 55.2 (OCH_3), 113.5 (C-3′ and C-5′), 120.0 (C-2″ and C-6″), 128.7 (C-3″ and C-5″), 129.1 (C-1″), 129.5 (C-2′ and C-6′), 130.7 (C-1′), 137.4 (C-4″), 161.9 (C-4′), 164.4 (C-4), 167.0 (C-6), 169.7 (C-2). Anal. calcd for $C_{17}H_{17}N_5O$: C, 66.43; H, 5.58; N, 22.79. Found: C, 66.32; H, 5.44; N, 22.68.

4.2.10. N^2-Phenyl-6-(3,4,5-trimethoxyphenyl)-1,3,5-triazine-2,4-diamine (10). Yield 48%. Mp 111–113 °C (EtOH). ^{1}H NMR (300 MHz, DMSO-d_6): δ 3.75 (3H, s, p-OCH_3), 3.87 (6H, s, m-$(OCH_3)_2$), 6.99 (1H, t, J = 7.3 Hz, H-4″), 7.11 (2H, brs, NH_2), 7.30 (2H, dd, J = 7.7 Hz, J = 8.1 Hz, H-3″ and H-5″), 7.68 (2H, s, H-2′ and H-6′), 7.85 (2H, dd, J = 0.9 Hz, J = 8.5 Hz, H-2″ and H-6″), 9.51 (1H, s, NH); ^{13}C NMR (75 MHz, DMSO-d_6): δ 55.8 (m-$(OCH_3)_2$), 60.0 (p-OCH_3), 105.0 (C-2″and C-6″), 119.9 (C-2′ and C-6′), 121.9 (C-1′), 128.3 (C-3′ and C-5′), 132.0 (C-1″), 139.9 (C-4′), 140.3 (C-4″), 152.6 (C-3″ and C-5″), 164.4 (C-4), 167.1 (C-6), 169.6 (C-2). Anal. calcd for $C_{18}H_{19}N_5O_3$: C, 61.18; H, 5.42; N, 19.82. Found: C, 60.96; H, 5.34; N, 19.67.

4.2.11. N^2-(2-Fluorophenyl)-6-(3,4,5-trimethoxyphenyl)-1,3,5-triazine-2,4-diamine (11). Yield 50%. Mp 177–179 °C (EtOH). ^{1}H NMR (300 MHz, DMSO-d_6): δ 3.74 (3H, p-OCH_3), 3.84 (6H, m-$(OCH_3)_2$), 7.07 (2H, brs, NH_2), 7.16–7.29 (3H, m, H-3″, H-4″ and H-5″), 7.64 (2H, s, H-2′ and H-6′), 7.78–7.84 (1H, m, H-6″), 9.03 (1H, s, NH); ^{13}C NMR (75 MHz, DMSO-d_6): δ 55.7 (m-$(OCH_3)_2$), 60.0 (p-OCH_3), 105.0 (C-2′ and C-6′), 115.4 (d, $^2J_{CF}$ = 19.4 Hz, C-3″), 123.9 (d, $^3J_{CF}$ = 3.4 Hz, C-4″), 125.3 (d, $^3J_{CF}$ = 8.4 Hz, C-6″), 126.5 (d, $^4J_{CF}$ = 1.5 Hz, C-5″), 126.7 (d, $^2J_{CF}$ = 10.8 Hz, C-1″), 131.9 (C-1′), 140.3 (C-4′), 152.5 (C-3′ and C-5′), 155.3 (d, $^1J_{CF}$ = 245.9 Hz, C-2″), 165.0 (C-4), 167.3 (C-6), 169.6 (C-2). Anal. calcd for $C_{18}H_{19}FN_5O_3$: C, 58.22; H, 4.89; N, 18.86. Found: C, 58.05; H, 4.79; N, 18.68.

4.2.12. N^2-(2-Chlorophenyl)-6-(3,4,5-trimethoxyphenyl)-1,3,5-triazine-2,4-diamine (12). Yield 43%. Mp 176–178 °C (EtOH). ^{1}H NMR (300 MHz, DMSO-d_6): δ 3.75 (3H, p-OCH_3), 3.84 (6H, m-$(OCH_3)_2$), 7.11 (2H, brs, NH_2), 7.19 (1H, ddd, J = 1.6 Hz, J = 7.6 Hz, J = 7.8 Hz, H-4″), 7.36 (1H, ddd, J = 1.3 Hz, J = 7.6 Hz, J = 7.8 Hz, H-5″), 7.51 (1H, dd, J = 1.4 Hz, J = 8.0 Hz, H-3″), 7.64 (2H, s, H-2′ and H-6′), 7.87 (1H, dd, J = 1.5 Hz, J = 8.1 Hz, H-6″), 8.80 (1H, s, NH); ^{13}C NMR (75 MHz, DMSO-d_6): δ 55.7 (m-$(OCH_3)_2$), 60.0 (p-OCH_3), 105.0 (C-2′ and C-6′), 125.8 (C-6″), 127.1 (C-2″ and C-4″), 127.9 (C-5″), 129.3 (C-3″), 131.8 (C-1′), 135.8 (C-1″), 140.4 (C-4′), 152.6 (C-3′ and C-5′), 165.0 (C-4), 167.3 (C-6), 169.7 (C-2). Anal. calcd for $C_{18}H_{19}ClN_5O_3$: C, 55.75; H, 4.68; N, 18.06. Found: C, 55.49; H, 4.57; N, 17.90.

4.2.13. N^2-(2-Methoxyphenyl)-6-(3,4,5-trimethoxyphenyl)-1,3,5-triazine-2,4-diamine (13). Yield 49%. Mp 173–175 °C (EtOH). ^{1}H NMR (300 MHz, DMSO-d_6): δ 3.75 (3H, p-OCH_3), 3.86 (9H, m-$(OCH_3)_2$ and o-OCH_3), 6.96 (1H, ddd, J = 4.2 Hz, J = 4.2 Hz, J = 8.4 Hz, H-4″), 7.05–7.07 (2H, m, H-3″ and H-5″), 7.15 (2H, brs, NH_2), 7.67 (2H, s, H-2′ and H-6′), 8.02 (1H, s, NH), 8.24 (1H, d, J = 7.5 Hz, H-6″); ^{13}C NMR (75 MHz, DMSO-d_6): δ 55.7 (o-OCH_3), 55.7 (m-$(OCH_3)_2$), 60.0 (p-OCH_3), 105.0 (C-2′ and C-6′), 110.9 (C-3″), 120.1 (C-5″), 122.0 (C-6″), 123.4 (C-4″), 127.8 (C-1″), 131.8 (C-1′), 140.4 (C-4′), 149.6 (C-2″), 152.6 (C-3′ and C-5′), 164.5 (C-4), 167.2 (C-6), 169.6 (C-2). Anal. calcd for $C_{19}H_{21}N_5O_4$: C, 59.52; H, 5.52; N, 18.27. Found: C, 59.42; H, 5.39; N, 18.05.

4.2.14. N^2-(3-Chlorophenyl)-6-(3,4,5-trimethoxyphenyl)-1,3,5-triazine-2,4-diamine (14). Yield 52%. Mp 193–195 °C (EtOH). ^{1}H NMR (300 MHz, DMSO-d_6): δ 3.76 (3H, p-OCH_3), 3.89 (6H, m-$(OCH_3)_2$), 7.03 (1H, ddd, J = 0.8 Hz, J = 2.0 Hz J = 8.0 Hz, H-4″), 7.24 (2H, br s, NH_2), 7.32 (1H, dd, J = 8.1 Hz, J = 8.1 Hz, H-5″), 7.67 (3H, m, H-6″, H-2′ and H-6′), 8.20 (1H, s, H-2″), 9.74 (1H, s, NH); ^{13}C NMR (75 MHz, DMSO-d_6): δ 55.8 (m-$(OCH_3)_2$), 60.1 (p-OCH_3), 105.0 (C-2′ and C-6′), 118.1 (C-6″), 119.1 (C-2″), 121.4 (C-1″), 129.9 (C-5″), 131.8 (C-1′), 132.8 (C-3″), 140.5 (C-4′), 141.6 (C-4″), 152.6 (C-3′ and C-5′), 164.4 (C-4), 167.0 (C-6), 169.8 (C-2). Anal. calcd for $C_{18}H_{19}ClN_5O_3$: C, 55.75; H, 4.68; N, 18.06. Found: C, 55.63; H, 4.54; N, 17.86.

4.2.15. N^2-(3-Methylphenyl)-6-(3,4,5-trimethoxyphenyl)-1,3,5-triazine-2,4-diamine (15). Yield 55%. Mp 192–194 °C (EtOH). ^{1}H NMR (300 MHz, DMSO-d_6): δ 2.31 (3H, s, CH_3), 3.76 (3H, p-OCH_3), 3.88 (6H, m-$(OCH_3)_2$), 6.82 (1H, d, J = 7.4 Hz, H-4″), 7.11 (2H, br s, NH_2), 7.18 (1H, dd, J = 7.8 Hz, J = 7.8 Hz, H-5″), 7.63 (1H, d, J = 8.4 Hz, H-6″), 7.71 (2H, s, H-2′ and H-6′), 7.75 (1H, s, H-2″), 9.44 (1H, s, NH); ^{13}C NMR (75 MHz, DMSO-d_6): δ 21.3 (CH_3), 55.8 (m-$(OCH_3)_2$), 60.1 (p-OCH_3), 105.0 (C-2′ and C-6′), 117.2 (C-6″), 120.5 (C-2″), 122.7 (C-1″), 128.1 (C-5″), 132.1 (C-1′), 137.4 (C-4″), 139.9 (C-3″), 140.4 (C-4′), 152.6 (C-3′ and C-5′), 164.5 (C-4), 167.1 (C-6), 169.6 (C-2). Anal. calcd for $C_{19}H_{21}N_5O_3$: C, 62.11; H, 5.76; N, 19.06. Found: C, 61.93; H, 5.64; N, 18.88.

4.2.16. N^2-(4-Chlorophenyl)-6-(3,4,5-trimethoxyphenyl)-1,3,5-triazine-2,4-diamine (16). Yield 53%. Mp 209–211 °C (EtOH). ^{1}H NMR (300 MHz, DMSO-d_6): δ 3.75 (3H, s, p-OCH_3), 3.87 (6H, s, m-$(OCH_3)_2$), 7.19 (2H, brs, NH_2), 7.35 (2H, d, J =

8.9 Hz, H-3″ and H-5″), 7.68 (2H, s, H-2′ and H-6′), 7.90 (2H, d, J = 8.9 Hz, H-2″ and H-6″), 9.67 (1H, s, NH); ^{13}C NMR (75 MHz, DMSO-d_6): δ 55.8 (m-$(OCH_3)_2$), 60.0 (p-OCH_3), 105.0 (C-2′ and C-6′), 121.2 (C-2″ and C-6″), 125.5 (C-1″), 128.1 (C-3″ and C-5″), 131.9 (C-1′), 139.0 (C-4″), 140.4 (C-4′), 152.6 (C-3′ and C-5′), 164.3 (C-4), 167.0 (C-6), 169.7 (C-2). Anal. calcd for $C_{18}H_{19}ClN_5O_3$: C, 55.75; H, 4.68; N, 18.06. Found: C, 55.62; H, 4.55; N, 17.94.

4.2.17. N^2-(4-Bromophenyl)-6-(3,4,5-trimethoxyphenyl)-1,3,5-triazine-2,4-diamine (17). Yield 61%. Mp 217–219 °C (EtOH). ^{1}H NMR (300 MHz, DMSO-d_6): δ 3.76 (3H, s, p-OCH_3), 3.87 (6H, s, m-$(OCH_3)_2$), 7.19 (2H, brs, NH_2), 7.47 (2H, d, J = 8.9 Hz, H-3″ and H-5″), 7.68 (2H, s, H-2′ and H-6′), 7.86 (2H, d, J = 8.9 Hz, H-2″ and H-6″), 9.68 (1H, s, NH); ^{13}C NMR (75 MHz, DMSO-d_6): δ 55.8 (m-$(OCH_3)_2$), 60.0 (p-OCH_3), 105.0 (C-2′ and C-6′), 113.4 (C-1″), 121.7 (C-2″ and C-6″), 131.0 (C-3″ and C-5″), 131.9 (C-1′), 139.4 (C-4″), 140.4 (C-4′), 152.6 (C-3′ and C-5′), 164.3 (C-4), 167.0 (C-6), 169.7 (C-2). Anal. calcd for $C_{18}H_{18}BrN_5O_3$: C, 50.01; H, 4.20; N, 16.20. Found: C, 49.85; H, 4.09; N, 16.03.

4.2.18. N^2-(4-Methylphenyl)-6-(3,4,5-trimethoxyphenyl)-1,3,5-triazine-2,4-diamine (18). Yield 55%. Mp 208–210 °C (EtOH). ^{1}H NMR (300 MHz, DMSO-d_6): δ 2.26 (3H, s, CH_3), 3.75 (3H, s, p-OCH_3), 3.86 (6H, s, m-$(OCH_3)_2$), 7.07 (2H, brs, NH_2), 7.10 (2H, d, J = 8.3 Hz, H-3″ and H-5″), 7.68 (2H, s, H-2′ and H-6′), 7.72 (2H, d, J = 8.3 Hz, H-2″ and H-6″), 9.41 (1H, s, NH); ^{13}C NMR (75 MHz, DMSO-d_6): δ 20.3 (CH_3), 55.7 (m-$(OCH_3)_2$), 60.0 (p-OCH_3), 105.0 (C-2′ and C-6′), 120.0 (C-2″and C-6″), 128.7 (C-3″ and C-5″), 130.8 (C-1″), 132.1 (C-1′), 137.3 (C-4″), 140.3 (C-4′), 152.6 (C-3′ and C-5′), 164.3 (C-4), 167.0 (C-6), 169.5 (C-2). Anal. calcd for $C_{19}H_{21}N_5O_3$: C, 62.11; H, 5.76; N, 19.06. Found: C, 61.97; H, 5.65; N, 18.91.

4.2.19. N^2-(4-Methoxyphenyl)-6-(3,4,5-trimethoxyphenyl)-1,3,5-triazine-2,4-diamine (19). Yield 52%. Mp 195–197 °C (EtOH). ^{1}H NMR (300 MHz, DMSO-d_6): δ 3.74 (3H, s, p-OCH_3), 3.75 (3H, s, p-OCH_3), 3.86 (6H, s, m-$(OCH_3)_2$), 6.89 (2H, d, J = 9.0 Hz, H-3″ and H-5″), 7.03 (2H, brs, NH_2), 7.68 (2H, s, H-2′ and H-6′), 7.71 (2H, d, J = 9.1 Hz, H-2″ and H-6″), 9.34 (1H, s, NH); ^{13}C NMR (75 MHz, DMSO-d_6): δ 55.1 (p-OCH_3), 55.7 (m-$(OCH_3)_2$), 60.0 (p-OCH_3), 104.9 (C-2′ and C-6′), 113.5 (C-3″ and C-5″), 121.7 (C-2″ and C-6″), 132.1 (C-1′), 132.9 (C-1″), 140.2 (C-4′), 152.5 (C-3′ and C-5′), 154.6 (C-4″), 164.3 (C-4), 167.1 (C-6), 169.4 (C-2). Anal. calcd for $C_{19}H_{21}N_5O_4$: C, 59.52; H, 5.52; N, 18.27. Found: C, 59.36; H, 5.44; N, 18.12.

4.2.20. N^2-(4-(Trifluoromethoxy)phenyl)-6-(3,4,5-trimethoxyphenyl)-1,3,5-triazine-2,4-diamine (20). Yield 56%. Mp 179–181 °C (EtOH). ^{1}H NMR (300 MHz, DMSO-d_6): δ 3.75 (3H, s, p-OCH_3), 3.87 (6H, s, m-$(OCH_3)_2$), 7.20 (2H, brs, NH_2), 7.30 (2H, d, J = 8.8 Hz, H-3″ and H-5″), 7.67 (2H, s, H-2′ and H-6′), 7.95 (2H, d, J = 9.1 Hz, H-2″ and H-6″), 9.72 (1H, s, NH); ^{13}C NMR (75 MHz, DMSO-d_6): δ 55.8 (m-$(OCH_3)_2$), 60.1 (p-OCH_3), 105.0 (C-2′ and C-6′), 120.2 (q, $^1J_{CF}$ = 255.1 Hz, OCF_3), 121.1 (C-3″ and C-5″), 121.2 (C-2″ and C-6″), 131.9 (C-1′), 139.2 (C-1″), 140.4 (C-4′), 142.7 (q, $^3J_{CF}$ = 1.7 Hz, C-4″), 152.6 (C-3′ and C-5′), 164.4 (C-4), 167.1 (C-6), 169.7 (C-2). Anal. calcd for $C_{19}H_{18}F_3N_5O_4$: C, 52.18; H, 4.15; N, 16.01. Found: C, 52.07; H, 4.08; N, 15.96.

4.2.21. N^2-(4-Isopropylphenyl)-6-(3,4,5-trimethoxyphenyl)-1,3,5-triazine-2,4-diamine (21). Yield 49%. Mp 190–192 °C (EtOH). ^{1}H NMR (300 MHz, DMSO-d_6): δ 1.20 (6H, d, J = 6.9 Hz, $CH(CH_3)_2$), 2.85 (1H, sept, J = 6.9 Hz, $CH(CH_3)_2$), 3.75 (3H, s, p-OCH_3), 3.87 (6H, s, m-$(OCH_3)_2$), 7.06 (2H, brs, NH_2), 7.16 (2H, d, J = 8.6 Hz, H-3″ and H-5″), 7.68 (2H, s, H-2′ and H-6′), 7.72 (2H, d, J = 8.6 Hz, H-2″ and H-6″), 9.41 (1H, s, NH); ^{13}C NMR (75 MHz, DMSO-d_6): δ 23.9 ($CH(\underline{C}H_3)_2$), 32.7 ($\underline{C}H(CH_3)_2$), 55.7 (m-$(OCH_3)_2$), 60.0 (p-OCH_3), 105.0 (C-2′ and C-6′), 120.3 (C-2″ and C-6″), 126.0 (C-3″ and C-5″), 132.1 (C-1′), 137.5 (C-1″), 140.3 (C-4′), 142.1 (C-4″), 152.6 (C-3′ and C-5′), 164.4 (C-4), 167.1 (C-6), 169.5 (C-2). Anal. calcd for $C_{21}H_{25}N_5O_3$: C, 63.78; H, 6.37; N, 17.71. Found: C, 63.65; H, 6.22; N, 17.54.

4.3. X-ray structure determination of 20

Intensity data for a colourless crystal of **20** (0.05 × 0.09 × 0.13 mm) were measured at 100 K on an XtaLAB Synergy Dual Atlas diffractometer equipped with a CCD area detector and graphite-monochromated Cu Kα radiation (λ = 1.54184 Å) so that θ_{max} = 67.1°. Data reduction and empirical absorption corrections, based on a multi-scan technique, were applied.[23] The structure was solved by direct methods[24] and refined on F^2 with anisotropic displacement parameters and C-bound H atoms in the riding model approximation.[25] The nitrogen-bound H atoms were refined with a distance restraint N–H = 0.88 ± 0.01 Å. A weighting scheme of the form $w = 1/[\sigma^2(F_o^2) + (0.104P)^2 + 1.179P]$ where $P = (F_o^2 + 2F_c^2)/3$ was introduced. The final refinement on 292 parameters yielded R = 0.059 (3044 data with $I \geq 2\sigma(I)$) and wR_2 = 0.176 (all 3357 data). The maximum and minimum residual electron density peaks of 1.73 and 0.62 eÅ^{-3}, respectively, were located 1.85 and 0.69 Å from the C19 and F1 atoms, respectively, that is, in chemically non-sensible positions. The molecular structure diagram was generated at the 70% probability level by ORTEP for Windows,[26] and the packing diagrams were generated with DIAMOND.[27] Additional analysis was conducted with PLATON.[28]

Crystal data for $C_{19}H_{18}F_3N_5O_4$: M = 437.38, triclinic, $P\bar{1}$, a = 7.2212(2), b = 10.9597(3), c = 13.4202(3) Å, α = 104.412(2)°, β = 99.253(2)°, γ = 108.517(2)°, V = 941.57(4) Å^3, Z = 2, D_x = 1.543 g cm^{-3}, $F(000)$ = 452 and μ = 1.125 mm^{-1}.

4.4. *In vitro* cytotoxicity assay

The synthesized compounds were tested against three breast tumor cell lines (MDA-MB231, SKBR-3 and MCF-7) and epithelial breast cell line (MCF-10A) by the MTT colorimetric assay.[29,30] All cells were obtained from the American Type Culture Collection. The cancerous cell lines were grown in Dulbecco's modified eagle medium (DMEM) supplemented with 10% fetal bovine serum (FBS) and 1% pen-strep antibiotic. The MCF-10A human epithelial breast cell line was grown in the complete mammary epithelial growth medium containing horse serum 5%, epithelial growth factor 20 ng mL^{-1}, hydrocortisone 0.5 mg mL^{-1}, cholera toxin 100 ng mL^{-1}, insulin 10 μg mL^{-1}, and pen-step antibiotic.[31] For the cytotoxic assay, 20 to 75 × 10^3 cells per mL (based on the doubling time for each cell line) were seeded in 96-well plates and the plates were incubated overnight in a humidified air atmosphere at 37 °C in 5% CO_2 incubator.

The cells were then treated with compounds at different concentrations. After 72 h of incubation, the MTT (0.5 mg mL^{-1}) was added to wells, followed by 4 h of incubation. The culture medium was then removed and DMSO (100 μL per well) was added and the absorbance values were measured at 570 nm using the multi-well Tecan NanoQuant, Infinite m200 Pro plate reader. Growth inhibitory values (GI_{50}) were calculated using GraphPad Prism 7 (GraphPad Software, San Diego, USA) by nonlinear regression analysis. Three independent experiments were carried out and the data was expressed in mean ± standard deviation (SD). The concentration–response curves used for the GI_{50} calculation are available in ESI.†

4.5. Time-dependent cytotoxicity

MDA-MB231 breast cancer cells were grown in DMEM supplemented with 10% FBS and 1% pen-strep antibiotic. The cells were seeded in 96-well plates (20×10^3 cells per mL) and the plates were incubated overnight in a humidified air atmosphere at 37 °C in 5% CO_2 incubator. The cells were then treated with compounds **16** or **18** in concentrations ranging from 0.2 nM to 125 nM for 12, 24, 48, and 72 h. After specified time for each experiment, MTT (0.5 mg mL^{-1}) was added to wells, followed by 4 h of incubation. The culture medium was then removed and DMSO (100 μL per well) was added and the absorbance values were measured at 570 nm using the multi-well Tecan NanoQuant, Infinite m200 Pro plate reader. GI_{50} values were calculated using GraphPad Prism 7 (GraphPad Software, San Diego, USA) by nonlinear regression analysis. All the time-dependent experiments at different times were carried out using the same passage of MDA-MB231 cells. Three independent experiments were carried out and the data were expressed in mean ± standard deviation (SD).

4.6. Acridine orange/propidium iodide staining

Fluorescence microscopy was used to visualize the apoptosis in cancer cells with AO/PI staining.[20] MDA-MB231 cells were grown in 6-well plate (5×10^5 cells per well). The cells were treated with respective compounds at concentrations equal to estimated GI_{20} and GI_{50} values and incubated for 24 h. One of the six wells was treated with 1% DMSO and served as a negative control, another well treated with methotrexate served as a positive control. After 24 h of incubation, the wells were washed with phosphate buffered saline (PBS) three times and 100 μL of AO (100 μg mL^{-1} in PBS) and 25 μL of PI (100 μg mL^{-1} in PBS) in 1 mL of media were added to each well. The plate was then observed under a motorized inverted fluorescent microscope (Eclipse Ti2-E, Nikon). Three independent experiments at each concentration were carried out.

4.7. Live cell imaging

MDA-MB231 cells (1×10^6 cells) were seeded in a Petri dish and incubated overnight in a humidified air atmosphere at 37 °C in 5% CO_2 incubator. Then, the Petri dish was washed with PBS three times and 300 μL of AO (100 μg mL^{-1} in PBS) and 75 μL of PI (100 μg mL^{-1} in PBS) in 3 mL of media were added to the Petri dish. The cells were treated with 10 μM of compound **18** and the dish was then transferred to motorized inverted fluorescent microscope (Eclipse Ti2-E, Nikon). The pictures were taken every 10 minutes for 4 h and intercalated into video (see ESI†).

4.8. QSAR model testing

The previously reported[16] 3D-QSAR model for 6,N^2-1,3,5-triazine-2,4-diamines against MDA-MB231 breast carcinoma was applied. The structures of the proposed compounds were drawn using ChemDraw 15.0 and imported to Discovery Studio v18 (ref. 32) for the activity prediction. The structures were prepared for the 3D-QSAR modeling and aligned to minimum energy using the 'align small molecules' protocol, which is based on 50% steric and 50% electrostatic fields for alignment of molecules. The predicted pGI_{50} values were then obtained by the 'calculate molecular properties' protocol in Discover Studio using the previously prepared 3D-QSAR model.

4.9. ADME properties prediction

QikProp module of the Schrodinger[33] was used to predict the absorption, distribution, metabolism and excretion (ADME) properties. The QikProp module predicts the descriptors which are pharmaceutically significant to identify the relevant properties of the organic molecule in relation to the 95% of the marketed drugs. The molecules were drawn and prepared (energy minimized and aligned) in Maestro program (v10.1) of Schrodinger software suit. QikProp (v4.3) was run with default options in normal processing mode.

Conflicts of interest

There are no conflicts to declare.

Acknowledgements

This work is supported by the Ministry of Higher Education, Malaysia under Fundamental Research Grant Scheme, grant number FRGS/1/2015/SG01/MUSM/03/1. This work received a partial support from the School of Pharmacy, Monash University Malaysia (Bridging Grant 2020). Sunway University Sdn Bhd is thanked for financial support of the X-ray crystallography laboratory (Grant No. STR-RCTR-RCCM-001-2019). Ahmad Junaid thanks Dr David Manallack and Monash University for the opportunity to carry out part of his research under the Vice Chancellor's International Intercampus PhD Mobility Scheme.

References

1 F. Bray, J. Ferlay, I. Soerjomataram, R. L. Siegel, L. A. Torre and A. Jemal, Global cancer statistics 2018: GLOBOCAN estimates of incidence and mortality worldwide for 36 cancers in 185 countries, *CA Cancer J. Clin.*, 2018, **68**, 394–424.

2 K. Polyak, Heterogeneity in breast cancer, *J. Clin. Invest.*, 2011, **121**, 3786–3788.

3 V. G. Kaklamani, A. L. Richardson and C. L. Arteaga, Exploring biomarkers of phosphoinositide 3-kinase pathway activation in the treatment of hormone receptor positive, human epidermal growth receptor 2 negative advanced breast cancer, *Oncologist*, 2019, **24**, 305–312.
4 N. M. Keegan, J. P. Gleeson, B. T. Hennessy and P. G. Morris, PI3K inhibition to overcome endocrine resistance in breast cancer, *Expert Opin. Invest. Drugs*, 2018, **27**, 1–15.
5 S. H. Hare and A. J. Harvey, mTOR function and therapeutic targeting in breast cancer, *Am. J. Cancer Res.*, 2017, **7**, 383–404.
6 C. Vicier, M. V. Dieci, M. Arnedos, S. Delaloge, P. Viens and F. Andre, Clinical development of mTOR inhibitors in breast cancer, *Breast Cancer Res.*, 2014, **16**, 203.
7 D. Kwapisz, Cyclin-dependent kinase 4/6 inhibitors in breast cancer: palbociclib, ribociclib, and abemaciclib, *Breast Cancer Res. Treat.*, 2017, **166**, 41–54.
8 D. Kwapisz, Cyclin-dependent kinase 4/6 inhibitors in hormone receptor-positive early breast cancer: preliminary results and ongoing studies, *Breast Cancer*, 2018, **25**, 506–516.
9 C. G. Murphy, The Role of CDK4/6 Inhibitors in Breast Cancer, *Current Treatment Options in Oncology*, 2019, **20**, 52.
10 J. Mehanna, F. G. Haddad, R. Eid, M. Lambertini and H. R. Kourie, Triple-negative breast cancer: current perspective on the evolving therapeutic landscape, *Int. J. Women's Health*, 2019, **11**, 431–437.
11 M. Robert, A. Patsouris, J. S. Frenel, C. Gourmelon, P. Augereau and M. Campone, Emerging PARP inhibitors for treating breast cancer, *Expert Opin. Emerging Drugs*, 2018, **23**, 211–221.
12 M. Younas, C. Hano, N. Giglioli-Guivarc'h and B. H. Abbasi, Mechanistic evaluation of phytochemicals in breast cancer remedy: current understanding and future perspectives, *RSC Adv.*, 2018, **8**, 29714–29744.
13 J. Liu, B. Ming, G.-H. Gong, D. Wang, G.-L. Bao and L.-J. Yu, Current research on anti-breast cancer synthetic compounds, *RSC Adv.*, 2018, **8**, 4386–4416.
14 S. Parvesh, N. Nomandla and K. Vipan, A review of the recent developments in synthetic anti-breast cancer agents, *Anti-Cancer Agents in Medicinal Chemistry*, 2016, **16**, 668–685.
15 S. Cascioferro, B. Parrino, V. Spanò, A. Carbone, A. Montalbano, P. Barraja, P. Diana and G. Cirrincione, 1,3,5-Triazines: a promising scaffold for anticancer drugs development, *Eur. J. Med. Chem.*, 2017, **142**, 523–549.
16 A. Junaid, F. P. L. Lim, L. H. Chuah and A. V. Dolzhenko, 6,N^2-Diaryl-1,3,5-triazine-2,4-diamines: synthesis, antiproliferative activity and 3D-QSAR modeling, *RSC Adv.*, 2020, **10**, 12135–12144.
17 A. Junaid and A. V. Dolzhenko, Microwave-assisted synthesis of 1,3,5-triazines: efficient approaches to therapeutically valuable scaffold, *Heterocycles*, 2019, **98**, 1678–1706.
18 A. Junaid, Y. S. Tan, E. R. T. Tiekink and A. V. Dolzhenko, A one-pot synthesis of N^2,6-diaryl-5,6-dihydro-1,3,5-triazine-2,4-diamines and systematic evaluation of their ability to host ethanol in crystals, *RSC Adv.*, 2019, **9**, 37660–37667.
19 A. Junaid, F. P. L. Lim, E. R. T. Tiekink and A. V. Dolzhenko, New one-pot synthesis of 1,3,5-triazines: three-component condensation, Dimroth rearrangement and dehydrogenative aromatization, *ACS Comb. Sci.*, 2019, **21**, 548–555.
20 D. Ribble, N. B. Goldstein, D. A. Norris and Y. G. Shellman, A simple technique for quantifying apoptosis in 96-well plates, *BMC Biotechnol.*, 2005, **5**, 12.
21 F. Lombardo, P. V. Desai, R. Arimoto, K. E. Desino, H. Fischer, C. E. Keefer, C. Petersson, S. Winiwarter and F. Broccatelli, In silico absorption, distribution, metabolism, excretion, and pharmacokinetics (ADME-PK): utility and best practices. An industry perspective from the international consortium for innovation through quality in pharmaceutical development, *J. Med. Chem.*, 2017, **60**, 9097–9113.
22 C. A. Lipinski, F. Lombardo, B. W. Dominy and P. J. Feeney, Experimental and computational approaches to estimate solubility and permeability in drug discovery and development settings, *Adv. Drug Delivery Rev.*, 2001, **46**, 3–26.
23 *CrysAlisPro*, Agilent Technologies, Santa Clara, CA (USA), 2013.
24 G. M. Sheldrick, A short history of SHELX, *Acta Crystallogr., Sect. A: Found. Adv.*, 2008, **64**, 112–122.
25 G. M. Sheldrick, Crystal structure refinement with SHELXL, *Acta Crystallogr., Sect. C: Struct. Chem.*, 2015, **71**, 3–8.
26 L. J. Farrugia, WinGX and ORTEP for Windows: an update, *J. Appl. Crystallogr.*, 2012, **45**, 849–854.
27 DIAMOND, *Visual Crystal Structure Information System, Version 3.1, CRYSTAL IMPACT*, Postfach 1251, D-53002, Bonn, Germany, 2006.
28 L. A. Spek, Structure validation in chemical crystallography, *Acta Crystallogr., Sect. D: Biol. Crystallogr.*, 2009, **65**, 148–155.
29 T. Mosmann, Rapid colorimetric assay for cellular growth and survival: application to proliferation and cytotoxicity assays, *J. Immunol. Methods*, 1983, **65**, 55–63.
30 D. A. Scudiero, R. H. Shoemaker, K. D. Paull, A. Monks, S. Tierney, T. H. Nofziger, M. J. Currens, D. Seniff and M. R. Boyd, Evaluation of a soluble tetrazolium/formazan assay for cell growth and drug sensitivity in culture using human and other tumor cell lines, *Cancer Res.*, 1988, **48**, 4827–4833.
31 J. Debnath, S. K. Muthuswamy and J. S. Brugge, Morphogenesis and oncogenesis of MCF-10A mammary epithelial acini grown in three-dimensional basement membrane cultures, *Methods*, 2003, **30**, 256–268.
32 D. S. Biovia, *Discovery studio modeling environment*, Dassault Systems, San Diego, 2017.
33 *QikProp, Version 4.3*, Schrödinger, LLC, New York, 2013.

